

## Effects of geometrical parameters on the performance of hydrogen regenerative pumps in proton exchange membrane fuel cell systems

Yuhang Chen<sup>a</sup>, Yutao Ling<sup>a</sup>, Anming Liu<sup>b</sup>, Lingzi Wang<sup>a,\*</sup>, Jianmei Feng<sup>a</sup>, Xueyuan Peng<sup>a,c</sup>

<sup>a</sup> School of Energy and Power Engineering, Xi'an Jiaotong University, Xi'an, 710049, Shaanxi, China

<sup>b</sup> China Automotive Engineering Research Institute Co., Ltd, Chongqing, 401122, China

<sup>c</sup> State Key Laboratory of Multiphase Flow in Power Engineering, Xi'an Jiaotong University, Xi'an, 710049, Shaanxi, China



### ARTICLE INFO

Handling Editor: Dr M Mahdi Najafpour

#### Keywords:

Regenerative pumps  
Hydrogen recirculation  
Proton exchange membrane fuel cell  
Numerical simulation

### ABSTRACT

Regenerative pumps are considered a promising option for hydrogen recirculation in proton exchange membrane fuel cell (PEMFC) systems. The geometry of the impeller exerts a direct influence on the pressurization process within the regenerative pumps. However, the influence has not been explored systematically in any available publications. This study investigates the effects of geometric parameters on pump performance and provides design guidelines for hydrogen regenerative pumps. A three-dimensional (3D) numerical model is developed and validated. The effects of critical geometric parameters, including the number of blades, impeller radius, and impeller radius ratio, on the performance of the regenerative pumps are then analyzed. Based on the analysis, this work recommends 35 blades and an impeller radius ratio of 0.65. To establish a correlation between operational performance and micro-flow mechanisms, the fluid velocity distribution at the interface of the rotating and stationary domains is quantitatively analyzed. Results indicate that a reduction in the flow rate results in increased axial velocity and decreased tangential velocity. The increased axial velocity enhances mass transfer, thus increasing the pressure and diminishing the efficiency, whereas the decreased tangential velocity intensifies the impact of the fluid on the blades, leading to increased shock losses and reduced efficiency.

### 1. Introduction

In recent years, the climate change and other environmental problems caused by the consumption of fossil fuels has aroused widespread concerns across different countries [1,2]. The necessity for the establishment of a clean and sustainable energy system is becoming increasingly apparent [3]. Currently, hydrogen energy is considered a low-carbon alternative to fossil fuels, offering several advantages, including cleanliness and high energy density [4–6]. Hydrogen fuel cell vehicles (HFCVs), recognized as zero-emission vehicles, represent a promising solution for harnessing hydrogen energy in the transportation sector [7,8].

The proton exchange membrane fuel cell (PEMFC) is an efficient energy conversion device that converts hydrogen energy into electricity, producing only water as by-products [9]. Due to its notable advantages, such as high efficiency, high power density, and good cold-start capabilities, PEMFC is considered superior for powering HFCVs [10,11]. In PEMFC systems, hydrogen is always supplied in excess of the requirement of the stack to optimize the output performance [12]. Therefore,

the anode hydrogen recirculation mode is preferred in PEMFC systems, because it improves the utilization of hydrogen and avoids water accumulation [13,14]. Hence, a reliable and efficient hydrogen recirculation component plays a crucial role in enhancing the performance and durability of PEMFC systems [15].

Hydrogen recirculation pumps and ejectors are two common components used to supply hydrogen to the fuel cell stacks [16]. As passive components, hydrogen recirculation ejectors have unique advantages in terms of reduced power consumption and increased efficiency. However, ejectors are prone to failure under low-power operating conditions and are susceptible to changes in operating conditions [17,18]. By contrast, hydrogen recirculation pumps have the prominent advantage of flow rate adjustment to accommodate variable operating conditions. Currently, scroll, claw, and roots pumps are the most widely used hydrogen recirculation pumps [19]. Nevertheless, inherent shortcomings, including manufacturing difficulties [20], contact wear [21], and knotty oil pollution [16], limit their prospects. Recently, regenerative pumps have gained traction in the hydrogen-recirculation pump market [22,23]. As dynamic compressors, regenerative pumps offer distinct

\* Corresponding author. School of Energy and Power Engineering, Xi'an Jiaotong University, 28 Xianning West Road, Xi'an, 710049, China.  
E-mail address: [wanglingzi@mail.xjtu.edu.cn](mailto:wanglingzi@mail.xjtu.edu.cn) (L. Wang).

advantages over other hydrogen recirculation pumps in terms of preventing oil pollution, avoiding wear problems and ensuring operational stability [24].

Regenerative pumps, also known as side channel pumps, have found applications in various industrial sectors, including chemical, petroleum, automobile, and power generation [25]. Their ability to transport high-pressure fluids at low flow rates enables them to replace positive-displacement compressors in certain applications [26]. In addition, regenerative machines offer various advantages, including simple construction, ease of manufacturing, low noise and vibration, and freedom from stall or surge instability [27]. Gessner [28] developed a four-stage helium regenerative compressor for use in cryogenic refrigerators for space vehicle applications. Regenerative compressors are used for natural gas compression in micro-turbine systems [29]. In addition, a regenerative compressor was selected as the secondary air pump to supply air to the exhaust system of an automotive engine to reduce emissions and improve the cold-start ability [30]. Although regenerative pumps have been employed in various applications, their use in hydrogen recirculation in PEMFC systems is relatively new, and relevant studies on this application are limited.

A concise one-dimensional (1D) prediction theory for hydrogen regenerative pumps was introduced [23]. This theory was used to predict the performance of a prototype designed by the FIAT Center of Research [24], and the theoretical predictions were in good agreement with the experimental results. The effects of leakage on the pump performance were then explored and integrated into an existing theoretical model [31]. Numerical simulations were also performed to analyze the internal flow mechanism and to verify the hypotheses proposed in the theoretical model [32]. Although existing studies cover both theories and experiments, the effects of geometric parameters on the performance of hydrogen regenerative pumps remain an unexplored area in the field of study.

Regenerative pumps have been applied in various fields, including the delivery of air, natural gas and helium. Based on their development, design guidelines for different regenerative machines have been proposed. For example, Raheel et al. [33] presented several detailed design criteria concerning the geometry of an impeller (e.g., number of blades and blade chevron angle). However, some results in Ref. [33] are inconsistent with those in Ref. [23] and with our findings, possibly due to the differences in the impeller shape and working fluid. Johanna et al. [34] revealed a qualitative relationship between two design parameters (head coefficient and blade angle) and pressurization performance. However, their study focused on air regenerative compressors with low rotational speeds and large sizes, thus offering limited guidance for hydrogen regenerative pumps. Feroskhan et al. [35] established several empirical correlations for regenerative machines based on extensive data from open publications. However, the application value is unsatisfactory due to a large error margin (15–25%). Due to the lack of relevant studies, the design of hydrogen regenerative pumps is limited.

Computational fluid dynamics (CFD) is a low-cost and efficient method for analyzing the internal flow of regenerative machines [36]. Jang [37] developed a three-dimensional (3D) steady-state numerical model for a two-stage regenerative compressor to verify an optimization method. A similar steady-state numerical model for a regenerative flow turbine in a small organic Rankine cycle system was developed by Moradi et al. [38]. Jeon et al. [39] designed a novel “S-shape” impeller for microbubble pumps and used ANSYS CFX to analyze the internal flow field and assess the performance. The handling method for the rotor in the aforementioned literature is the steady-state frozen-rotor approach. In addition, Insinna et al. [40] conducted steady and transient simulations of a regenerative pump. The transient method provides more detailed information on flow deviation prediction but is time-consuming. Based on the available publications, the widely used steady-state model with the frozen-rotor method is sufficiently accurate to predict the overall performance of regenerative machines [41,42].

In summary, regenerative pumps offer significant advantages for

hydrogen recirculation in PEMFC systems. However, a research gap exists in the existing literature regarding geometric parameters and design methods for hydrogen regenerative pumps. In the present paper, the effects of key geometric parameters, including the number of blades, impeller radius, and impeller radius ratio, on the operational performance of hydrogen regenerative pumps are studied. The performance curves of different models are compared, and the optimal number of blades and impeller radius ratio are proposed to provide design guidelines for engineers. To explain the pressurization principle and variation rule of performance curves, the internal flow velocities distribution on the interface of rotating and stationary domains is quantitatively analyzed.

## 2. Numerical model

### 2.1. Geometric model

**Fig. 1(a)** shows the overall structure of the hydrogen regenerative pump, which primarily consists of an impeller and casing. The inlet and outlet ports are machined on the casing and connected to the fluid channel, which is called the side channel. The cross section of the side channel and impeller is illustrated in **Fig. 1(b)**. In this model, the cross-sectional shapes of the side channel and vane are semi-circular. **Fig. 1(c)** shows the structure of the casing, where a stripper between the inlet and outlet is observed and the angle of the stripper is defined as  $\theta$ . When the pressurized fluid encounters the stripper, most of it exits from the discharge port, whereas only a small amount of it flows back to the inlet through a tiny clearance between the impeller and casing, as shown in **Fig. 1(d)**. Peripheral leakage through the stripper clearance contributes significantly to leakage losses, resulting in additional power consumption and reduced overall efficiency. To minimize leakage, the axial clearance is typically designed less than 0.6 mm [31].

The performance of a regenerative pump depends on various factors, including the geometric parameters, rotational speed, and fluid types. This investigation focuses on the effects of three key geometric parameters, namely, impeller radius  $r$  ( $r_0$ ), impeller radius ratio  $\epsilon$  ( $r_i/r_0$ ) and the number of blades  $Z$ . These three parameters collectively determine the impeller structure. The range for each parameter is defined based on practical applications and existing studies. Common hydrogen-recirculation pump products are generally no larger than 270 mm [43], and regenerative types are usually smaller. The impeller radius is constrained to the range of 50–90 mm, which meets the installation requirements of most fuel cell stacks. When the impeller radius is fixed, the impeller radius ratio determines the side channel cross-section area and has a direct influence on the performance curve. Typically, the value of impeller radius ratio is between 0.5 and 0.8 [25] and the research scope of this paper is 0.55–0.75. The kinetic energy is transferred to fluid by the blades, and the number of blades is a key parameter that determines the pressure rise and efficiency [44]. There is no conclusion to select the optimal number of blades. So six different numbers of blades (25–75) are studied to seek for an optimal number of blades. The geometric parameters of the models are listed in **Table 1**. The other parameters are fixed for all models, where the blade thickness is 1 mm, axial clearance  $\delta$  is 0.2 mm, and stripper angle  $\theta$  is 50°. The radii of inlet and outlet ports are the same with the blade height. A uniform nomenclature scheme is used to identify different models. For example, model 1 is denoted as model  $r50_{\epsilon}0.65_Z25$ , indicating a model with impeller radius  $r = 50$  mm, impeller radius ratio  $\epsilon = 0.65$  and number of blades  $Z = 25$ .

Different 3D models are generated based on the given parameters, and computational domains are extracted. **Fig. 2(a)** shows the computational domain of model  $r50_{\epsilon}0.65_Z25$ , which consists of a stationary and rotating domain, that are connected by an interface. The stationary domain encompasses the inlet and outlet tubes and the side channel. The rotating domain includes the blade grooves and an axial clearance that connects the adjacent blade grooves.

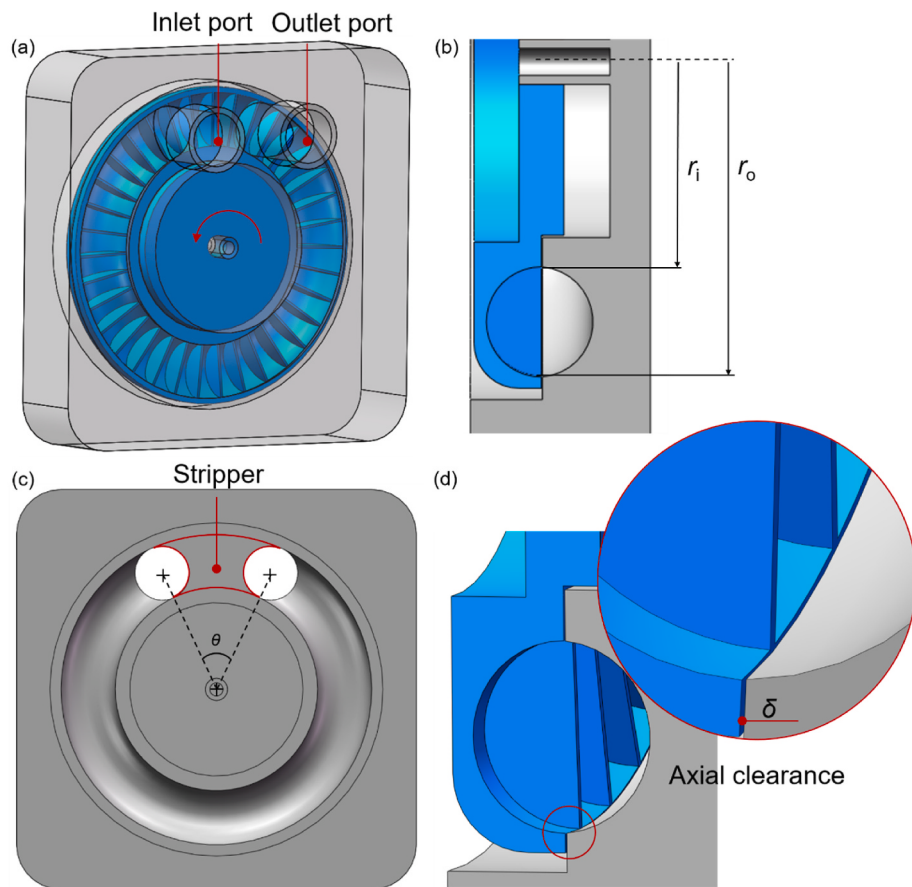


**Fig. 1.** Configuration of a hydrogen regenerative pump: (a) overview of the model; (b) cross-section of the model; (c) casing; (d) cross-section of the fluid channel.

**Table 1**  
Geometric parameters of studied models.

Name	r (mm)	$\epsilon$	Z
Model 1–16	50	0.65	25,35,45,55,65,75
Model 7–12	70	0.65	
Model 13–18	90	0.65	
Model 19–24	70	0.55	
Model 25–30	70	0.75	

## 2.2. Mesh generation and numerical settings

A structured hexahedral mesh was generated for the computational domain using ANSYS ICEM CFD v221. The grid of the rotating domain and stationary domain are generated separately, and merged together before numerical calculation. Fig. 2(a) shows the 3D mesh of model  $r50\_e0.65\_Z25$ , and Fig. 2(b) provides a cross-sectional view of the fluid channel, showing the grid details. In Fig. 2(b), the left mesh represents the rotating domain, whereas the right mesh represents the stationary

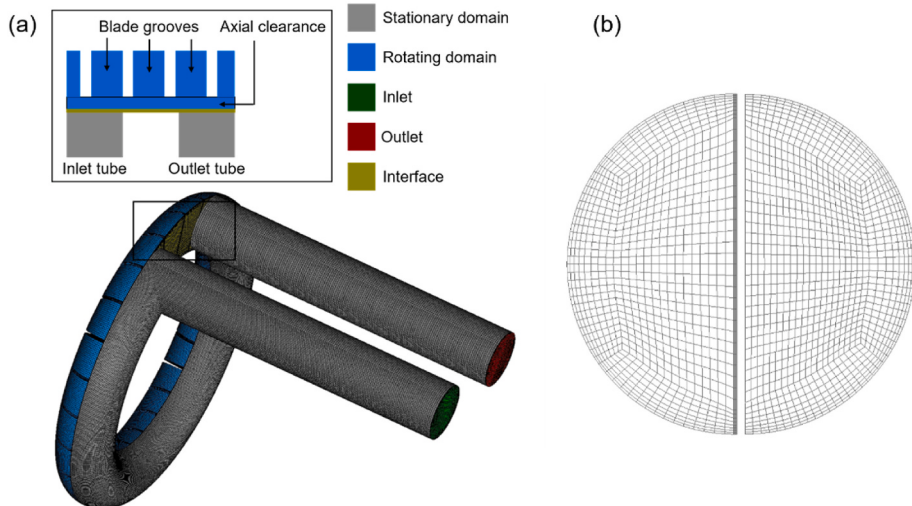


**Fig. 2.** Structured computational domain of model  $r50\_e0.65\_Z25$ : (a) overview of the computational domain; (b) grids in the cross section of fluid channel.

domain. In order to improve the stability of data transmission, the two parts are given similar mesh size on the contact interface. To ensure the calculation accuracy, five layers were generated for with an axial clearance of 0.2 mm. In addition, eight layers of cells were established for inflation near the wall. The mesh orthogonal quality and skewness were checked with a minimum orthogonal quality of 0.55 and maximum skewness of 0.6.

Three-dimensional Reynolds averaged Navier-Stokes simulations were performed using ANSYS CFX Solver v221. A steady-state approach was adopted, and the frozen-rotor option was used for the domain interface to simulate impeller rotation. Ideal hydrogen gas was used as the working fluid. The  $k-\omega$  shear-stress transport turbulence model with a 5% turbulent intensity was adopted [25]. The simulation applied the velocity-pressure coupling algorithm. In practical applications, the rotational speed typically ranges from 5000 to 25,000 rpm [23]. For this simulation, the rotational speed was set to 15,000 rpm. According to the actual working conditions, the inlet total pressure was set to 200 kPa and the inlet static temperature was 70 °C [45]. The outlet conditions were specified based on the variable mass flow rates.

### 2.3. Grid-independence verification and experiment validation

A grid-independence study was conducted before the batch simulation. For model *r50\_e0.65\_Z25*, four meshes with different global cell sizes were generated. The numbers of cells in the four meshes were  $0.5 \times 10^6$ ,  $1 \times 10^6$ ,  $2 \times 10^6$  and  $4 \times 10^6$ , respectively. Three mass flow rates were set for the grid-independence study. Isentropic efficiency  $\eta_{is}$  was chosen as the observed variable, which contains convergence information for both pressure and temperature. The isentropic efficiency variation trend against mass flow rate across different meshes is presented in Fig. 3. The results with the  $0.5 \times 10^6$  and  $1.0 \times 10^6$  cells exhibited significant deviations from the other two. Because the time cost and calculation accuracy were comprehensively considered, the mesh with  $2.0 \times 10^6$  cells was deemed appropriate for subsequent simulations. Thus, the global cell size of the mesh with  $2.0 \times 10^6$  cells was adopted for all other models.

A preparatory simulation was conducted to validate the numerical model. The geometric model and operating conditions were identical to those used in the experiment [23]. A comparison between the CFD results and reference data is presented in Fig. 4, revealing a maximum deviation of 4.3% and mean deviation of 2.3%. Notably, the CFD curve exhibits a lower slope than the experimental curve, which could be attributed to model simplification. The numerical model simplified all filleted corners, which affected the machine performance. In addition,

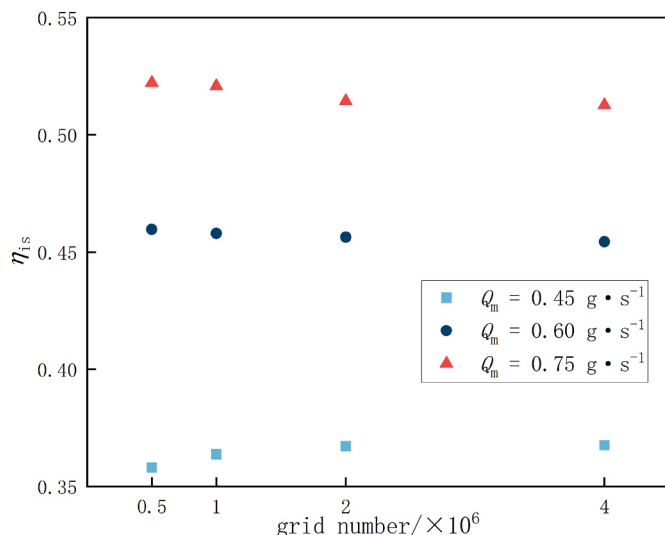


Fig. 3. Isentropic efficiency against mass flow rate for different meshes.

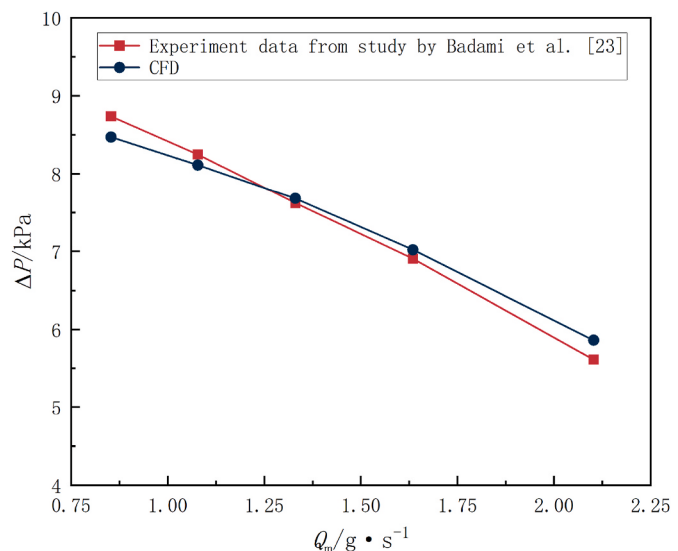


Fig. 4. Comparison of the CFD results and the experiment data from the study by Badami et al. [23].

the radial clearance was neglected in the numerical model. Based on the available references, the simulation results meet the practical requirements.

## 3. Results and discussion

The performance of pumps was evaluated under the two thermal parameters, pressure rise  $\Delta P$  and isentropic efficiency  $\eta_{is}$ . Pressure rise  $\Delta P$  is the static pressure increment from inlet to outlet and is a key parameter in PEMFC systems [46]. Isentropic efficiency  $\eta_{is}$  is a common and valid parameter to assess the compression process. The performance of regenerative machines is closely related to the impeller linear speed and side channel cross-sectional area [47]. Thus, dimensionless pressure coefficients  $\psi$  and flow coefficient  $\varphi$  are adopted when pumps with different impeller radius and side channel cross-section areas are compared. The calculation equations for these parameters are listed in Table 2.

### 3.1. Effects of the number of blades Z

The performance curves of the models with the same impeller radius ratio (0.65) but different impeller radii (50, 70 and 90 mm) are shown in Fig. 5. Models with the same impeller radius but different numbers of blades are compared in each subgraph. A similar trend was observed across the subgraphs; that is, when the flow rate was low, models with fewer blades had an obviously higher increase in pressure, whereas the efficiency remained practically the same. When the flow rate was high, models with different numbers of blades exhibited similar pressure, whereas the difference in efficiency was considerable.

Table 2  
Calculations of performance parameters.

Name	Symbol	Definition
Pressure rise Isentropic efficiency	$\Delta P$ $\eta_{is}$	$\frac{P_o - P_i}{(P_o/P_i)^{(r-1)/r} - 1}$
Dimensionless flow coefficient	$\varphi$	$\frac{T_o}{T_i} - 1$
Dimensionless pressure coefficient	$\psi$	$\frac{Q_v}{u_o A_c}$
		$\frac{\Delta P}{\frac{1}{2} \rho_i u_o^2}$

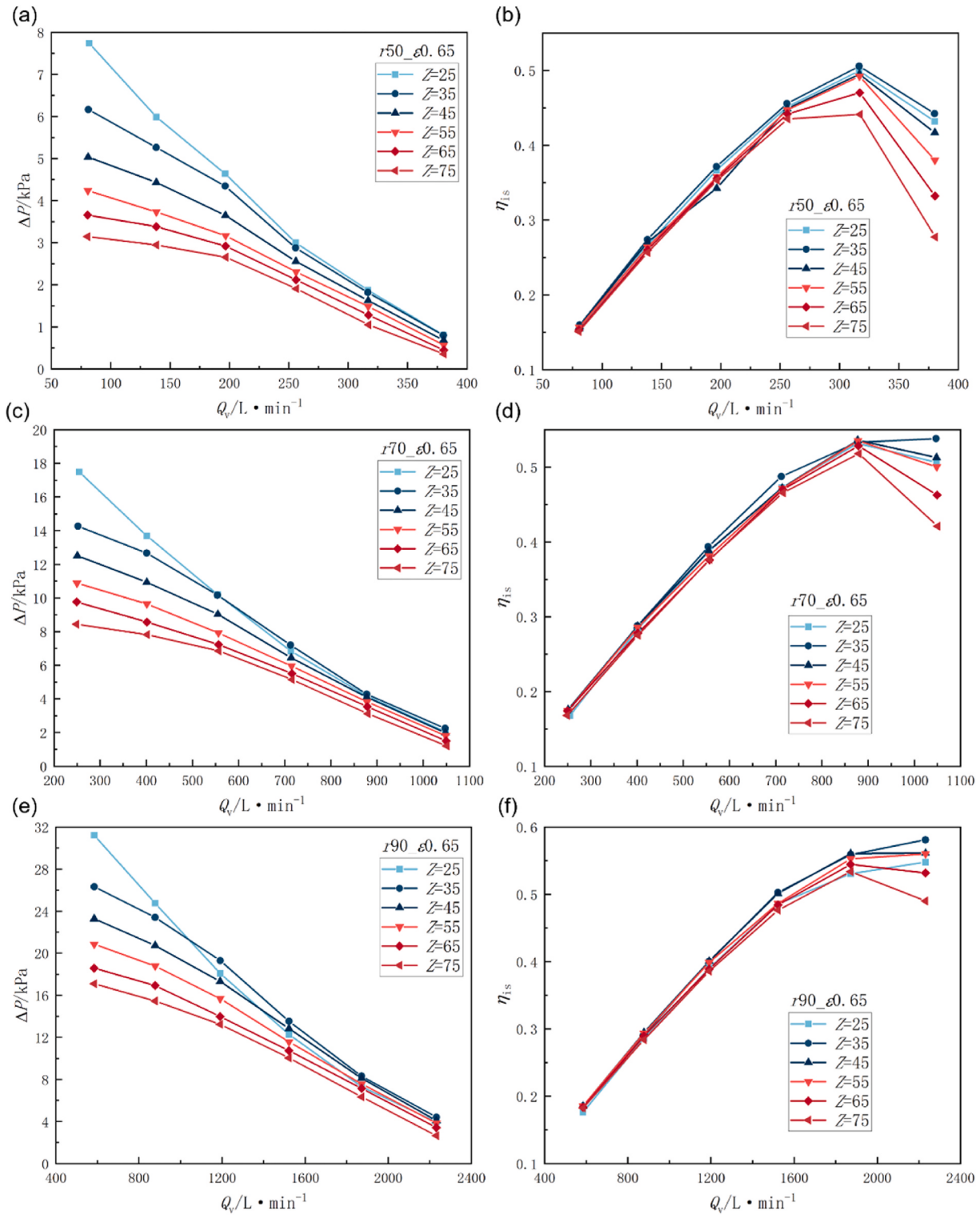


**Fig. 5.** Performance curves of models  $r50\text{--}90_{\varepsilon0.65}$ : (a), (c), (e): pressure rise against volume flow rate; (b), (d), (f): efficiency against volume flow rate.

**Fig. 5(a), (c), and (e)** show that model Z25 exhibited the highest pressure rise at low flow rates. However, as the flow rate increased, the pressure of model Z25 rapidly dropped and approached or even fell below that of model Z35. When the number of blades exceeded 35, the pressure declined with an increase in the number of blades. Model Z35 demonstrated a stable and satisfactory performance across a wide range of operations. **Fig. 5(b), (d), and (f)** show that model Z35 exhibited the highest efficiency at different flow rates. Therefore, within the scope of

our study ( $r50\text{--}90_{\varepsilon0.65}$ ), the number of blades for hydrogen regenerative pumps should be 35.

A closer examination of **Fig. 5** shows that the flow rate corresponding to the maximum efficiency point was also influenced by the number of blades. **Fig. 5(f)** shows that model  $r90_{\varepsilon0.65}$ , Z75 reached its peak efficiency at  $Q_v = 1900 \text{ L} \cdot \text{min}^{-1}$ , whereas model  $r90_{\varepsilon0.65}$ , Z35 reached it at  $Q_v = 2230 \text{ L} \cdot \text{min}^{-1}$ . An identical variation trend is observed in **Fig. 5(d)**. Therefore, it can be inferred that a higher number of blades not only

causes a decrease in pressure and efficiency, but also reduces the flow rate corresponding to the maximum efficiency point.

Fig. 6 shows the pressure and isentropic efficiency variation curves of the models with the same impeller radius (70 mm) but different impeller radius ratios (0.55, 0.65, and 0.75). Fig. 6(a) and (c) clearly show that model Z25 had the highest pressure at low flow rates. However, the advantage of the pressurization of model Z25 diminished gradually with increasing flow rates. Fig. 6(e) shows that the pressure of model Z25 at

low flow rates was lower than that of model Z35, which differs from Fig. 6(a) and (c). This discrepancy suggests that models with fewer blades exhibit poorer performance at high impeller radius ratios. Overall, model Z35 exhibited a superior pressurization performance under different conditions. Fig. 6(b), (d), and (f) show that model Z35 exhibited the highest efficiency across different flow rates. Therefore, the recommended number of blades remains 35 within the scope of our study ( $r70\_e0.55\text{--}0.75$ ).

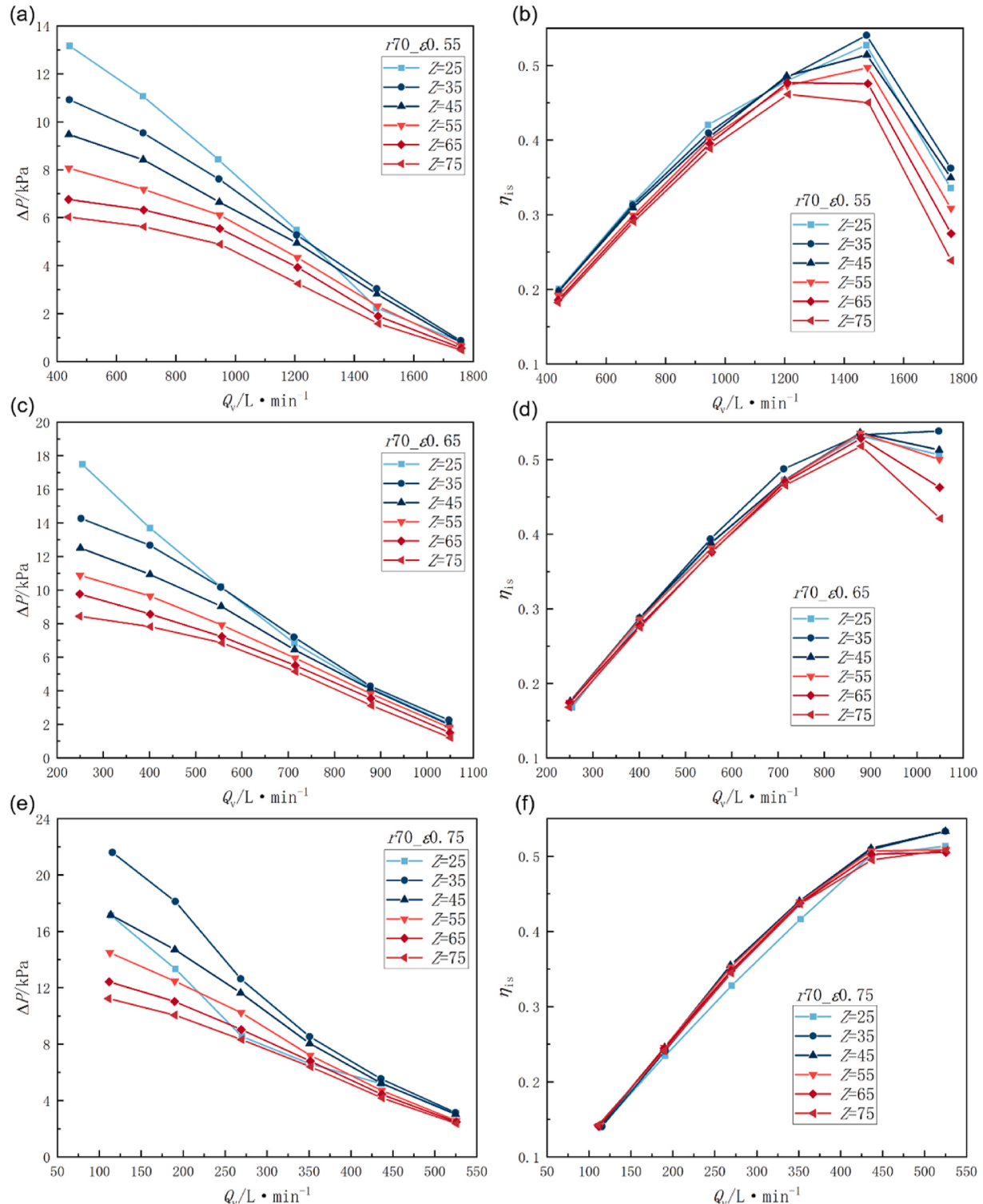


**Fig. 6.** Performance curves of models  $r70\_e0.55\text{--}0.75$ : (a), (c), (e): pressure rise against volume flow rate; (b), (d), (f): efficiency against volume flow rate.

Notably, Fig. 6(f) shows that the efficiency curve of model  $r70_{\varepsilon}0.75$ \_Z35 coincides with that of  $r70_{\varepsilon}0.75$ \_Z45. However, as shown in Fig. 6(b) and (d), models Z45 had lower efficiency than that of model Z35. Therefore, it can be speculated that if the impeller radius ratio continues to increase (exceeding 0.75), the optimal number of blades should also increase.

### 3.2. Effects of impeller radius $r$ and radius ratio $\varepsilon$

This section focuses on the effects of the impeller radius and impeller radius ratio on the overall performance, assuming a fixed number of 35 blades.

The dimensionless pressure coefficients and efficiency curves for models with different impeller radii are shown in Fig. 7. Throughout the entire operating range, the pressure coefficient increased with the impeller radius. The efficiencies of the different models were similar at low flow rates. However, as the flow rate increased, the models with longer radii exhibited higher efficiencies. With pressure and efficiency considered, longer impeller radii clearly lead to improved performance. In practical applications, the impeller radius is constrained by various factors such as installation space, impeller fatigue strength, and motor torque. Most importantly, the impeller size should correspond to the operating conditions at the design point. The data presented in Figs. 5 and 6 serve as a valuable reference for preliminary impeller design. If multiple impeller radii meet the operational requirements, the longer radius is chosen.

The dimensionless pressure coefficients and efficiency curves of the models with different impeller radius ratios are shown in Fig. 8. Notably, the pressure coefficient increased with impeller radius ratio, particularly at low flow rates. The effects of the impeller radius ratio on efficiency was significant. Model  $r70_{\varepsilon}0.55$  exhibited an efficiency curve similar to that of model  $r70_{\varepsilon}0.65$  when the dimensionless flow coefficient was less than 0.56. Nevertheless, as the dimensionless flow coefficient increased continuously, the efficiency of model  $r70_{\varepsilon}0.55$  declined sharply, whereas that of model  $r70_{\varepsilon}0.65$  increased slightly. The efficiency curve of model  $r70_{\varepsilon}0.75$  remained consistently lower than that of model  $r70_{\varepsilon}0.65$  within the entire flow rate range. However, these two curves intersected at the point where the dimensionless flow coefficient was 0.66. The efficiency curve of model  $r70_{\varepsilon}0.75$  may have surpassed that of model  $r70_{\varepsilon}0.65$  as the flow rate continued to increase. However, this working range is meaningless for practical applications because of the extremely low pressure.

In summary, increasing the impeller radius ratio is conducive to increasing pressure. However, when the impeller radius ratio exceeds

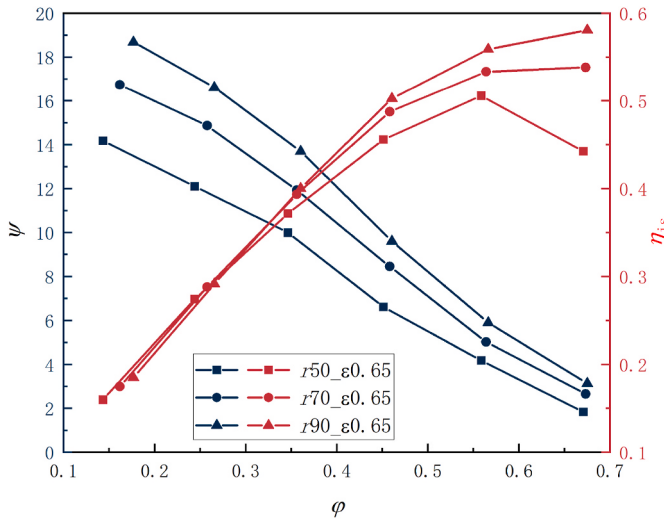


Fig. 7. Dimensionless performance curves for models  $r50$ – $90_{\varepsilon}0.65$ \_Z35.

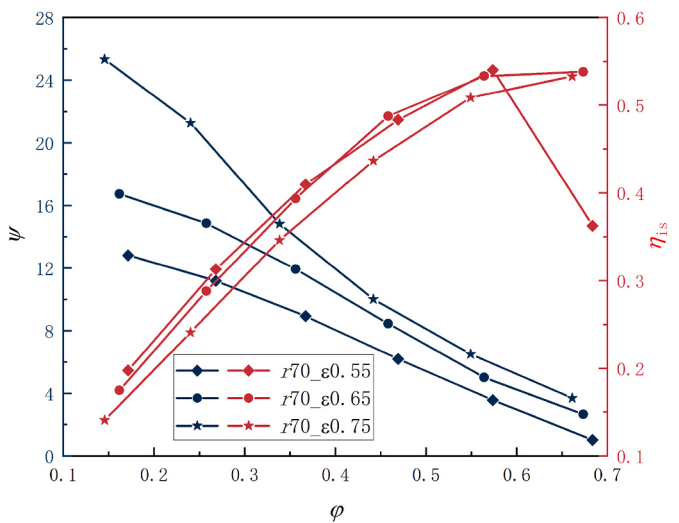


Fig. 8. Dimensionless performance curves for models  $r70_{\varepsilon}0.55$ – $0.75$ \_Z35.

0.65, the efficiency decreases. Therefore, the recommended value of the impeller radius ratio is approximately 0.65, which provides both high efficiency and a stable pressure. In special cases in which a high pressure is required, a higher impeller radius ratio is recommended.

### 3.3. Internal flow velocity distribution

Fig. 9(a) visualizes the helical flow path of the fluid through streamlines on the side channel wall. As the fluid spirals forward along the side channel, kinetic energy is transferred from the impeller to the fluid and is then converted to pressure energy within the side channel. After several circulations, the pressurized fluid moves toward the outlet and is expelled. Fig. 9(b) illustrates the fluid velocity vector on cross-section A-A. Due to centrifugal force, the fluid at point 1 accelerates along the blade groove and reaches point 2 at a high speed. The high-speed fluid then enters the side channel and mixes with the low-speed fluid, thereby increasing the static pressure. In an ideal single circulation, the energy increment is calculated by

$$W = h_2 - h_1 + \frac{c_2^2 - c_1^2}{2} \quad (3-1)$$

$$c_{1,2}^2 = c_{1,2,ax}^2 + c_{1,2,tan}^2 \quad (3-2)$$

where  $h_1$  and  $h_2$  denote the fluid enthalpy at points 1 and 2, respectively. Because points 1 and 2 are close in temperature and enthalpy,  $W$  is determined mainly by  $c_1$  and  $c_2$ . In practical scenarios, fluid absolute velocity  $c$  consists of three components: axial, tangential and radial velocities. Axial velocity is related to mass transfer between the rotating and stationary domains. Tangential velocity has the same direction as impeller linear velocity and is associated with the kinetic energy increment in a single circulation. Fig. 9(b) shows that the radial velocity is insignificant and therefore is not considered in Eq. (3-2). Consequently, the operational performance closely depends on the velocity distribution along the dividing line of the rotating and stationary domains (red line in Fig. 9(b)).

To conduct a quantitative analysis of the internal flow velocities, 100 points along the dividing line were extracted, and both the axial and tangential velocities at each point were counted. To assess comprehensively the effects of velocity distribution on the performance, the performance curves and internal velocity distribution curves of models  $r70_{\varepsilon}0.65$ \_Z35–75 are examined simultaneously. Fig. 10 illustrates the performance curves of models  $r70_{\varepsilon}0.65$ \_Z35–75. Although the variation patterns of the performance curves are discussed in Section 3.1, the current focus is on establishing the intrinsic relationship between the

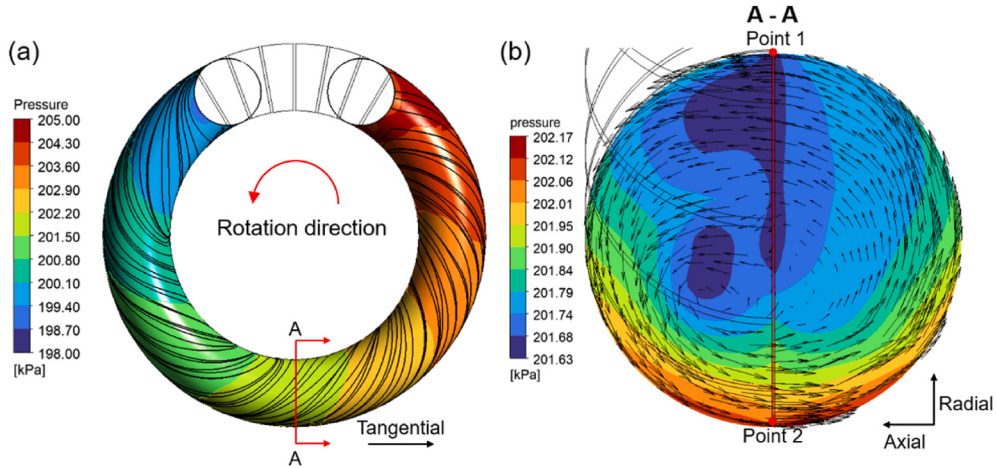


**Fig. 9.** Internal flow schematic of model *r70\_e0.65\_Z35* under the condition that volume flow rate = 877 L min<sup>-1</sup>: (a) streamline and pressure contour on the side channel wall; (b) velocity vector and pressure contour on the cross section of the fluid channel.

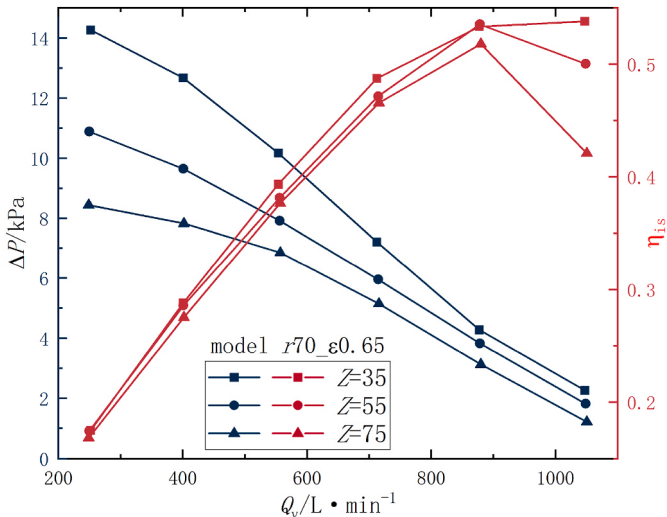


**Fig. 10.** Performance curves of models *r70\_e0.65\_Z35–75*.

performance curves and internal flow characteristics.

**Fig. 11** depicts the quantitative distributions of axial and tangential velocities along dividing line of model *r70\_e0.65\_Z35–75*. In **Fig. 11(a)**—a positive axial velocity indicates that the fluid flows from the impeller toward the side channel. In **Fig. 11(b)**—a positive tangential velocity indicates fluid movement in alignment with the direction of the impeller movement.

**Fig. 10** shows that the pressure diminished as the volume flow rate increased. This is a typical pressure–variation curve of regenerative machines [48]. Although some researchers have proposed several 1D theories to explain this characteristic [49,50], only a few used a 3D visualization method to explicate the flow mechanism. This problem is discussed from a microscopic perspective through numerical simulations. **Fig. 11** shows that as the volume flow rate increased, there was a concurrent decrease in axial velocity and an increase in tangential velocity, where the former significantly weakened the mass transfer process, thereby reducing the transmitted energy. In addition, according to Eq. (3-1) and Eq. (3-2), pressurization was also affected by  $c_1$  and  $c_2$ :

$$W = c_{2,ax}^2 - c_{1,ax}^2 + c_{2,tan}^2 - c_{1,tan}^2 \quad (3-3)$$

where **Table 3** lists the calculated average values for each variable in Eq. (3-3). **Table 3** also shows the decreases in axial velocity and increases in

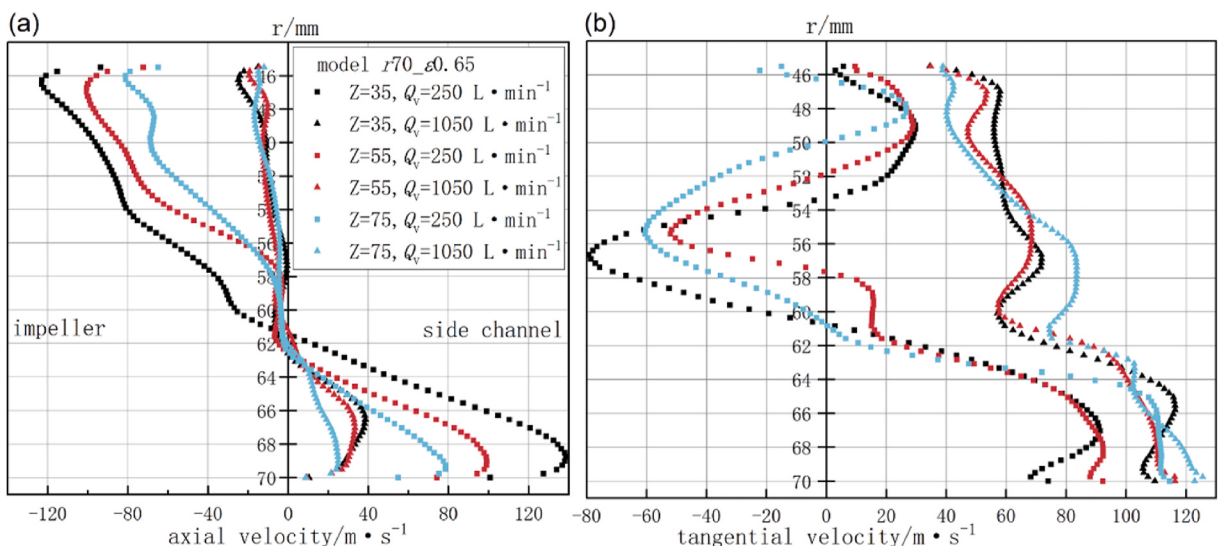


**Fig. 11.** Velocity distribution curves on the dividing line of models *r70\_e0.65\_Z35–75*: (a) axial velocity distribution; (b) tangential velocity distribution.

**Table 3**  
Average values of velocity components and specific work.

$Q_v$	Z	$c_{1,ax}$	$c_{2,ax}$	$c_{1,tan}$	$c_{2,tan}$	$W$
250	—			$m \cdot s^{-1}$		
	35	-73	84	-12	71	6625
	55	-49	60	-14	79	7244
1050	75	-38	43	-18	98	9685
	35	-8	25	60	108	8625
	55	-9	20	58	103	7564
	75	-8	15	62	109	8198

tangential velocity with increasing flow rates. The relationship between the specific work  $W$  and flow rates  $Q_v$  is irregular. In other words, the flow rate had little effect on the specific work within a single circulation. However, as the flow rate increased, the average tangential velocity increased, thereby reducing the number of circulations of fluid, which adversely affected pressurization. This is why the pressure decreased with increasing flow rates.

Fig. 11(b) shows that the negative tangential velocity values were observed at low flow rates, indicating that backflow occurred. The backflow intensified the impact of the fluid on the blades and increased shock losses. This explains the extremely low efficiency at low flow rates. Another reason is violent mass transfer at low flow rates. Fig. 11(a) shows that the axial velocity was quite high at low flow rates, enhancing the mass transfer between the impeller and side channel. Although mass transfer is the core principle of pressurization for regenerative machines, it concurrently causes a complex flow pattern and increases flow losses. Thus, the efficiency and pressure cannot coincide in regenerative machines.

Models with varying numbers of blades are compared in Fig. 10. As the number of blades increased, the pressure and efficiency decreased. Fig. 11(a) shows that when the volume flow rate was  $1050 \text{ L min}^{-1}$ , models with different numbers of blades exhibited similar axial velocity distributions. When the volume flow rate was  $250 \text{ L min}^{-1}$ , the greater the number of blades, the lower was the axial velocity, which weakened the mass transfer. Although the specific work increased with the number of blades at a volume flow rate of  $250 \text{ L min}^{-1}$ , the enhanced pressurization was counteracted by the decrease in axial velocity and a weak mass transfer. In addition, the increased tangential velocity reduced the number of fluid circulations of fluid. This is why an increase in the number of blades had adverse effects on pressurization.

The number of blades also affects the operational efficiency. An increase in the number of blades reduces the effective flow area within the interface and enhances the blockage effect, leading to a decrease in axial velocity and pressure. In addition, the increased number of blades increases the likelihood of fluid impacting the blades, further reducing the efficiency.

#### 4. Conclusion

In this study, the influence of the number of blades, impeller radius, and impeller radius ratio on the performance of hydrogen regenerative pumps was evaluated via numerical simulation. Optimal geometric parameter values were determined by analyzing the performance curves of 30 models. Furthermore, a quantitative analysis of the internal velocity distribution was performed to reveal the micro-flow mechanism. The main conclusions are as follows.

- 1) An optimal number of blades for hydrogen regenerative pumps could be identified, where a number that was greater or less than this optimal number diminished the pressure and reduced efficiency. The recommended number of blades is 35 within the scope of our study (impeller radius: 50–70 mm, impeller radius ratio: 0.55–0.75).
- 2) Increasing the impeller radius resulted in higher pressure and efficiency. Because different impeller radii correspond to different flow and pressure ranges, an appropriate impeller radius can be

determined under a given operational condition. Fig. 5 serves as a crucial reference for determining the impeller radius.

- 3) The pressure increased with the impeller radius ratio. However, when the impeller radius ratio exceeded 0.65, the efficiency decreased. The recommended value of the impeller radius ratio was approximately 0.65. In situations requiring high pressure, a larger impeller radius ratio is recommended.
- 4) As the flow rate decreased, the axial velocity increased and the tangential velocity decreased. The increased axial velocity enhanced mass transfer, thereby elevating the pressure and reducing efficiency. The decreased tangential velocity intensified the impact of the fluid on the blades, further reducing efficiency.

The regenerative pumps represent a novel type of hydrogen recirculation pumps with promising potential. It is necessary to carry out continuous and in-depth studies on it. The future research will focus on the improvement of impeller structure to enhance the pump performance. In addition, the combined utilization of regenerative pumps and ejectors is a significant issue as well.

#### Nomenclature

Symbols	
$A_c$	Side channel cross-section area [ $\text{m}^2$ ]
$c$	Fluid absolute velocity [ $\text{m s}^{-1}$ ]
$h$	Enthalpy of fluid [ $\text{J kg}^{-1}$ ]
$n$	Rotational speed [rev $\text{min}^{-1}$ ]
$P$	Pressure [Pa]
$\Delta P$	Pressure rise from inlet to outlet [Pa]
$Q_v$	Volume flow rate [ $\text{m}^3 \text{s}^{-1}$ ]
$Q_m$	Mass flow rate [ $\text{g s}^{-1}$ ]
$r$	Impeller radius [m]
$T$	Temperature [K]
$u$	Impeller tangential velocity [ $\text{m s}^{-1}$ ]
$W$	Specific work [ $\text{m}^2 \text{s}^{-2}$ ]
$Z$	Impeller blade number [–]
Greek symbols	
$\gamma$	Isentropic exponent [–]
$\delta$	Axial clearance [mm]
$\varepsilon$	Impeller radius ratio [–]
$\eta_{is}$	Isentropic efficiency [–]
$\theta$	Stripper angle [ $^\circ$ ]
$\rho$	Gas density [ $\text{kg m}^{-3}$ ]
$\varphi$	Dimensionless flow coefficient [–]
$\psi$	Dimensionless pressure coefficient [–]
$\omega$	Angular speed of impeller [rad $\text{s}^{-1}$ ]
Subscripts	
ax	Axial
b	Blade
i	Inner/inlet
o	Outer/outlet
tan	Tangential

#### CRediT authorship contribution statement

**Yuhang Chen:** Writing – original draft. **Yutao Ling:** Investigation. **Anming Liu:** Resources. **Lingzi Wang:** Writing – review & editing. **Jianmei Feng:** Supervision. **Xueyuan Peng:** Project administration.

#### Declaration of competing interest

The authors declare that they have no known competing financial interests or personal relationships that could have appeared to influence the work reported in this paper.

#### Acknowledgments

This research was supported by the National Key Research and Development Program of China [Grant No. 2021YFB2500500].

## References

- [1] Hoang AT, Pham VV, Nguyen XP. Integrating renewable sources into energy system for smart city as a sagacious strategy towards clean and sustainable process. *J Clean Prod* 2021;305. <https://doi.org/10.1016/j.jclepro.2021.127161>.
- [2] Tarafdar A, Sowmya G, Yogeshwari K, Rattu G, Negi T, Awasthi MK, et al. Environmental pollution mitigation through utilization of carbon dioxide by microalgae. *Environ Pollut* 2023;328. <https://doi.org/10.1016/j.envpol.2023.121623>.
- [3] Islam A, Islam T, Mahmud H, Raihan O, Islam MS, Marwani HM, et al. Accelerating the green hydrogen revolution: a comprehensive analysis of technological advancements and policy interventions. *Int J Hydrogen Energy* 2024;67:458–86. <https://doi.org/10.1016/j.ijhydene.2024.04.142>.
- [4] Bodkhe RG, Shrivastava RL, Soni VK, Chadge RB. A review of renewable hydrogen generation and proton exchange membrane fuel cell technology for sustainable energy development. *Int J Electrochem Sci* 2023;18. <https://doi.org/10.1016/j.ijoes.2023.100108>.
- [5] Liu Q, Lan F, Chen J, Zeng C, Wang J. A review of proton exchange membrane fuel cell water management: membrane electrode assembly. *J Power Sources* 2022;517. <https://doi.org/10.1016/j.jpowsour.2021.230723>.
- [6] Asghar R, Hassan S, Yaqoob Y. A comprehensive overview of wet chemistry methodologies and their application in the fabrication of materials for PEM fuel cell. *Int J Hydrogen Energy* 2024;58:1190–203. <https://doi.org/10.1016/j.ijhydene.2024.01.289>.
- [7] Andrade TS, Thiringer T. From hydrogen fuel to wheels: characterizing the powertrain hydrogen/energy consumption for battery versus hydrogen fuel cell vehicle. In: 2023 IEEE IAS global conference on renewable energy and hydrogen technologies (GlobConHT); 2023. p. 1–5. <https://doi.org/10.1109/GlobConHT56829.2023.10087509>.
- [8] Knibbe R, Harding D, Burton J, Cooper E, Amir Zadeh Z, Sagulenko M, et al. Optimal battery and hydrogen fuel cell sizing in heavy-haul locomotives. *J Energy Storage* 2023;71. <https://doi.org/10.1016/j.est.2023.108090>.
- [9] Edwards H, Pereira MP, Gharai S, Omrani R, Shabani B. Computational fluid dynamics modelling of proton exchange membrane fuel cells: accuracy and time efficiency. *Int J Hydrogen Energy* 2024;50:682–710. <https://doi.org/10.1016/j.ijhydene.2023.09.004>.
- [10] Aminudin MA, Kamarudin SK, Lim BH, Majilan EH, Masdar MS, Shaari N. An overview: current progress on hydrogen fuel cell vehicles. *Int J Hydrogen Energy* 2023;48:4371–88. <https://doi.org/10.1016/j.ijhydene.2022.10.156>.
- [11] Luo Y, Jiao K. Cold start of proton exchange membrane fuel cell. *Prog Energy Combust Sci* 2018;64:29–61. <https://doi.org/10.1016/j.pecs.2017.10.003>.
- [12] Zhang Q, Feng J, Wen J, Peng X. 3D transient CFD modelling of a scroll-type hydrogen pump used in FCVs. *Int J Hydrogen Energy* 2018;43:19231–41. <https://doi.org/10.1016/j.ijhydene.2018.08.158>.
- [13] Steinberger M, Geiling J, Oechsner R, Frey L. Anode recirculation and purge strategies for PEM fuel cell operation with diluted hydrogen feed gas. *Appl Energy* 2018;232:572–82. <https://doi.org/10.1016/j.apenergy.2018.10.004>.
- [14] Grimm M, Hellmann M, Kemmer H, Kabelac S. Interaction of cell flow directions and performance in PEM fuel cell systems following an anode based water management approach. *J Power Sources* 2023;580. <https://doi.org/10.1016/j.jpowsour.2023.233270>.
- [15] Yu X, Fan J, Zhou Y, Hao D, Chen J, Yu T, et al. Experimental investigation of the effect of hydrogen recirculation on the performance of a proton exchange membrane fuel cell. *Int J Hydrogen Energy* 2022;47:1183–91. <https://doi.org/10.1016/j.ijhydene.2021.10.063>.
- [16] Han J, Feng J, Chen P, Liu Y, Peng X. A review of key components of hydrogen recirculation subsystem for fuel cell vehicles. *Energy Convers Manag X* 2022;15. <https://doi.org/10.1016/j.ecmx.2022.100265>.
- [17] Yang Y, Du W, Ma T, Lin W, Cong M, Yang H, et al. Numerical studies on ejector structure optimization and performance prediction based on a novel pressure drop model for proton exchange membrane fuel cell anode. *Int J Hydrogen Energy* 2020;45:23343–52. <https://doi.org/10.1016/j.ijhydene.2020.06.068>.
- [18] Han J, Feng J, Hou T, Peng X. Performance investigation of a multi-nozzle ejector for proton exchange membrane fuel cell system. *Int J Energy Res* 2020;45:3031–48. <https://doi.org/10.1002/er.5996>.
- [19] Liang X, Kang H, Shen J, Li Z, Zeng R. Review and analysis of hydrogen recirculation devices for compact vehicular proton exchange membrane fuel cells. *J Power Sources* 2023;555. <https://doi.org/10.1016/j.jpowsour.2022.232308>.
- [20] Hsieh C-F, Hwang Y-W, Fong Z-H. Study on the tooth profile for the screw claw-type pump. *Mech Mach Theor* 2008;43:812–28. <https://doi.org/10.1016/j.mechmachtheory.2007.06.011>.
- [21] Jianmei F, Qingqing Z, Tianfang H, Xueyuan P. Dynamics characteristics analysis of the oil-free scroll hydrogen recirculating pump based on multibody dynamics simulation. *Int J Hydrogen Energy* 2021;46:5699–713. <https://doi.org/10.1016/j.ijhydene.2020.11.065>.
- [22] Ma K, Liu Y, Wei Z, Yang J, Guo B. A novel high-speed permanent magnet synchronous motor for hydrogen recirculation side channel pumps in fuel cell systems. *Energies* 2022;15. <https://doi.org/10.3390/en15238913>.
- [23] Badami M, Mura M. Theoretical model with experimental validation of a regenerative blower for hydrogen recirculation in a PEM fuel cell system. *Energy Convers Manag* 2010;51:553–60. <https://doi.org/10.1016/j.enconman.2009.10.022>.
- [24] Badami M, Mura M. Setup and validation of a regenerative compressor model applied to different devices. *Energy Convers Manag* 2011;52:2157–64. <https://doi.org/10.1016/j.enconman.2010.10.044>.
- [25] Sreekanth M, Sivakumar R, Sai Santosh Pavan Kumar M, Karunamurthy K, Shyam Kumar MB, Harish R. Regenerative flow pumps, blowers and compressors – a review. *Proc Inst Mech Eng A J Power Energy* 2021;235:1992–2013. <https://doi.org/10.1177/09576509211018118>.
- [26] Raheel M, Engeda A, Hamrin D, Rouse G. The performance characteristics of single-stage and multistage regenerative flow compressors for natural gas compression application. *Proc IME C J Mech Eng Sci* 2003;217:1221–39.
- [27] Raheel M, Engeda A. Current status, design and performance trends for the regenerative flow compressors and pumps. In: ASME international mechanical engineering congress and exposition; 2002. p. 99–110.
- [28] Multistage Gessner R. gas-bearing, helium compressor development. In: *Advances in cryogenic engineering: proceedings of the 1966 cryogenic engineering conference university of Colorado engineering research center and cryogenics division NBS institute for materials research boulder, Colorado june 13–15, 1966*. Springer; 1967. p. 631–9.
- [29] Raheel M, Engeda A. Performance characteristics of regenerative flow compressors for natural gas compression application. *J Energy Resour Technol* 2005;127:7–14.
- [30] Engeda A, Elkacimi Y. A regenerative flow compressor as a secondary air pump for engine emission control. *Proc IME C J Mech Eng Sci* 2008;222:1707–15. <https://doi.org/10.1243/09540462jmes958>.
- [31] Badami M, Mura M. Leakage effects on the performance characteristics of a regenerative blower for the hydrogen recirculation of a PEM fuel cell. *Energy Convers Manag* 2012;55:20–5. <https://doi.org/10.1016/j.enconman.2011.10.002>.
- [32] Badami M, Mura M. Comparison between 3D and 1D simulations of a regenerative blower for fuel cell applications. *Energy Convers Manag* 2012;55:93–100. <https://doi.org/10.1016/j.enconman.2011.10.003>.
- [33] Raheel MM, Engeda A. Systematic design approach for radial blade regenerative turbomachines. *J Propul Power* 2005;21:884–92. <https://doi.org/10.2514/1.1426>.
- [34] Adam J, Heinrich M, Schwarze R. Influence of different design parameters on side channel compressor performance. *Fortsch Im Ingenieurwes* 2022;86:819–27. <https://doi.org/10.1007/s10010-022-00594-y>.
- [35] M F, M S, K K, R S, Sinaga N, Khan TMY. Regression-analysis-based empirical correlations to design regenerative flow machines. *Energies* 2022;15. <https://doi.org/10.3390/en15113861>.
- [36] Zhang F, Chen K, Appiah D, Hu B, Yuan S, Asomani SN. Numerical delineation of 3D unsteady flow fields in side channel pumps for engineering processes. *Energies* 2019;12. <https://doi.org/10.3390/en12071287>.
- [37] Jang C-M, Han G-Y. Enhancement of performance by blade optimization in two-stage ring blower. *J Therm Sci* 2010;19:383–9. <https://doi.org/10.1007/s11630-010-0398-5>.
- [38] Moradi R, Habib E, Bocci E, Cioccolanti L. Investigation on the use of a novel regenerative flow turbine in a micro-scale Organic Rankine Cycle unit. *Energy* 2020;210. <https://doi.org/10.1016/j.energy.2020.118519>.
- [39] Jeon S-Y, Yoon J-Y, Jang C-M. Optimal design of a novel 'S-shape' impeller blade for a microbubble pump. *Energies* 2019;12. <https://doi.org/10.3390/en12091793>.
- [40] Insinna M, Salvadori S, Martelli F, Peroni G, Simon G, Dipace A, et al. One-dimensional prediction and three-dimensional CFD simulation of the fluid dynamics of regenerative pumps. In: *Turbo expo: power for land, sea, and air*. American Society of Mechanical Engineers; 2018. V02CT42A036.
- [41] Nejad J, Riasi A, Nourbakhsh A. Parametric study and performance improvement of regenerative flow pump considering the modification in blade and casing geometry. *Int J Numer Methods Heat Fluid Flow* 2017;27:1887–906. <https://doi.org/10.1108/hff-03-2016-0088>.
- [42] Quail F, Scanlon T, Stickland M. Design optimisation of a regenerative pump using numerical and experimental techniques. *Int J Numer Methods Heat Fluid Flow* 2011;21:95–111. <https://doi.org/10.1108/0961553111095094>.
- [43] Gao Y, Lin M. Research on the performance characteristics of hydrogen circulation pumps for PEMFC vehicles. *Int J Hydrogen Energy* 2024;50:1255–72. <https://doi.org/10.1016/j.ijhydene.2023.10.248>.
- [44] Fleder A, Böhle M. A systematical study of the influence of blade number on the performance of a side channel pump. *J Fluid Eng* 2019;141. <https://doi.org/10.1115/1.4043166>.
- [45] Kong X, Han J, Guo Y, Feng J, Peng X. Investigation on the pressure fluctuation of hydrogen Roots pump with a novel reflow structure for fuel cell vehicles. *Int J Hydrogen Energy* 2024;50:66–78. <https://doi.org/10.1016/j.ijhydene.2023.08.021>.
- [46] Guo Y, Wiebe W, Unwerth Tv, Schmitz S. Hydrogen pump for hydrogen recirculation in fuel cell vehicles. *E3S Web of Conferences* 2020;155. <https://doi.org/10.1051/e3sconf/202015501001>.
- [47] Fleder A, Böhle M. A systematical study of the influence of blade length, blade width, and side channel height on the performance of a side channel pump. *J Fluid Eng* 2015;137. <https://doi.org/10.1115/1.4030897>.
- [48] Brown A. A comparison of regenerative and centrifugal compressors. In: *International compressor engineering conference*; 1972.
- [49] Song J, Engeda A, Chung MK. A modified theory for the flow mechanism in a regenerative flow pump. *Proc Inst Mech Eng A J Power Energy* 2003;217:311–21.
- [50] Yoo IS, Park MR, Chung MK. Improved momentum exchange theory for incompressible regenerative turbomachines. *Proc Inst Mech Eng A J Power Energy* 2006;219:567–81. <https://doi.org/10.1243/095765005x31252>.